

Two New Polymorphs of the Organic Semiconductor 9,10-Diphenylanthracene: Raman and X-ray Analysis

Tommaso Salzillo,[†] Raffaele Guido Della Valle,[†] Elisabetta Venuti,^{*,†} Aldo Brillante,[†] Theo Siegrist,[‡] Matteo Masino,[§] Francesco Mezzadri,[§] and Alberto Girlando^{*,§}

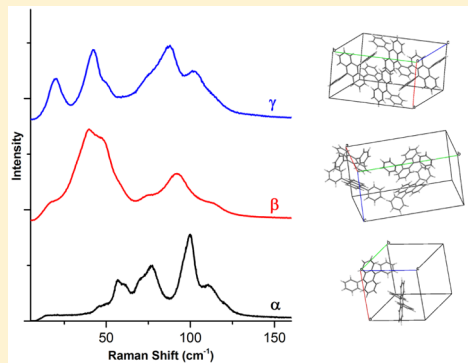
[†]Dip. di Chimica Industriale “Toso Montanari” and INSTM-UdR Bologna, Università di Bologna, Viale Risorgimento 4, I-40136 Bologna, Italy

[‡]Dept. of Chemical and Biomedical Engineering, FAMU-FSU College of Engineering, Florida State University and Florida A&M University, Tallahassee, Florida 32310-6046, United States

[§]Dip. di Chimica and INSTM-UdR Parma, Università degli Studi di Parma, Area delle Scienze 17/A, I-43124 Parma, Italy

S Supporting Information

ABSTRACT: Raman microscopy in the lattice phonon region coupled with X-ray diffraction have been used to study the polymorphism in crystals and microcrystals of the organic semiconductor 9,10-diphenylanthracene (DPA) obtained by various methods. While solution grown specimens all display the well-known monoclinic structure widely reported in the literature, by varying the growth conditions two more polymorphs have been obtained, either from the melt or by sublimation. By injecting water as a nonsolvent in a DPA solution, one of the two new polymorphs was predominantly obtained in the shape of microribbons. Lattice energy calculations allow us to assess the relative thermodynamic stability of the polymorphs and verify that the energies of the different phases are very sensitive to the details of the molecular geometry adopted in the solid state. The mobility channels of DPA polymorphs are shortly investigated.



INTRODUCTION

Among the continuously growing family of organic semiconductors,¹ 9,10-diphenylanthracene (DPA) occupies a peculiar place, as it is one of the few crystals exhibiting good hole and electron mobility.² DPA is also an highly fluorescent material, representing a useful building block for optoelectronic devices.³ In addition, and at variance with many organics, DPA is characterized by good chemical stability and a melting point around 522 K, well above the operating temperature of electronic devices. Besides, it melts without decomposition, making it possible to obtain an high degree of purification by zone refining.²

It is indisputable that high chemical purity is a key factor to achieve reproducible intrinsic carrier mobilities in organics. However, it has been shown that in these systems charge transport also dramatically depends on the polymorphic phase of the compound. In fact, different polymorphs may correspond to different molecular packings in the crystal, thus to altogether different hopping integrals between the orbitals responsible for the charge carrier mobilities.^{4–8} Furthermore, the possible coexistence of more solid phases in a sample (phase mixing)⁹ is an intrinsic source of disorder and has detrimental effects on the mobility.¹⁰ Indeed, despite the fact that the phenomenon of polymorphism in molecular crystals has attracted attention of pharmaceutical research for a long time,¹¹ only recently has

there been an increasing interest for it in the field of small molecule organic semiconductors.^{12–14}

As for DPA, three X-ray determinations from solution grown crystals (under different conditions) have been reported, all giving the same $C2/c$ structure.^{15–17} An old private communication reports that crystals grown from the melt belong to a different ($P2/m$) structure, for which only cell parameters were given.¹⁸ Highly pure crystals grown by Bridgman's method (i.e., the melt), on which hole and electron mobilities were measured,² were however found to have the same structure as the solution grown ones.² Also nanocrystals have been reported to belong to the same $C2/c$ structure.^{19,20}

Then apparently the situation of DPA polymorphism looks settled, apart from an old report.¹⁸ Notwithstanding, we felt that investigation on possible DPA polymorphism required a more systematic approach: in view of the varied possible applications of this compound, one needs to know the number of its polymorphs, the way each of them can be obtained, and their relative thermodynamic stability. We have therefore grown DPA crystals by different methods, including nanocrystallization²¹ and vapor phase sublimation, which is known to produce crystals of good quality. We have then used low-frequency

Received: November 12, 2015

Revised: December 29, 2015

Raman spectroscopy^{9,12} to single out and separate the polymorphs, subsequently characterized by X-ray diffraction (XRD). In this way we have been able to identify three different DPA polymorphs, named hereafter α , β , and γ . Polymorph α is the well-known form grown from solution, found in commercial DPA, and corresponds to that obtained by Bridgman's technique. The β and γ polymorphs have similar unit cell parameters but different crystal structures ($P2_1/a$ and $P2_1/n$) and are often obtained together by sublimation or from the melt. We have also found that microribbons obtained from solution mainly correspond to the β polymorph.²¹ Lattice dynamics calculations allow us to ascertain the relative thermodynamic stability of the three phases, and the computation of the hopping integrals provides a basis to correlate the intrinsic transport properties to the molecular packings.

METHODS

Sample Preparation. DPA (purity 99%) was purchased from Aldrich. The procedures to obtain the crystals were as follows: (1) Slow evaporation of a toluene solution in a 2 mL vial at ambient conditions yielded needlelike crystals a few millimeters long, always belonging to the α polymorph, as the original commercial product. (2) DPA microcrystals were grown at room temperature by injecting 100 μ L of a 2×10^{-3} M solution of DPA in THF in 5 mL of Milli-Q water under vigorous stirring.²¹ The sample was kept stirring for 3 min and then left overnight to allow for the crystal growth. The crystals obtained in this way have the shape of ribbons \approx 40 μ m long, with aspect ratios around 40:1. They belong to the β polymorph. (3) Small single crystals of various morphologies, all belonging to the γ phase, were obtained from recrystallized DPA, by melting it in a vial and letting it cool down to room temperature. The vapor condensed on the walls of the same vial formed colorless plateletlike crystals of the β polymorph. (4) A setup similar to the one described previously²² was used to produce vapor phase transport²³ grown DPA crystals. A gas stream of argon or forming gas is utilized to transport DPA molecules from the source zone at elevated temperature into a shallow temperature gradient growth zone. The obtained crystals were transparent flat platelets of millimetric size of either the β or the γ polymorph. (5) Single crystals of the γ polymorph were also obtained by sublimation at 160 °C at low pressure (10 Pa) of N₂, and at the optical microscope they appeared like platelets of elongated irregular shape. In the same growth, it was possible to identify and select for the measurements needle crystals of the α polymorph.

Experimental Setup. Raman spectra have been obtained by a Jobin Yvon T6400 triple monochromator spectrometer, interfaced to a Olympus BX40 microscope. The Jobin Yvon confocality allowed for a spatial resolution of the order of 1 μ m, with a theoretical field depth in the range from 7 to 25 μ m, depending on the microscopy objective. The Raman excitation was from a krypton laser tuned at 647.1 nm, keeping the power at the sample of the order of 1–2 mW to avoid damage of the sample.

XRD analysis of vapor grown crystals was performed by using an Oxford Diffraction Xcalibur2 CCD diffractometer with graphite monochromated Mo K α radiation. For temperature control, an Oxford Instruments Cryojet cold nitrogen stream system was used. Data collections were carried out at temperatures of 105, 200, and 295 K. Data reduction used the Oxford Diffraction CRYSTALIS suite of programs. An

absorption correction was applied to the observed intensities. All subsequent calculations were carried out using the program CRYSTALS,²⁴ with SIR92²⁵ to provide the starting solution for the structure refinement. Single crystal XRD data of differently grown crystals were collected with Mo K α radiation on a Bruker AXS Smart diffractometer, equipped with an APEX II CCD area-detector. The structure was solved using SIR2004²⁵ and refined full-matrix with SHELLX97²⁶ making use of anisotropic thermal parameters for all atoms except hydrogen.

Powder XRD data were collected using Cu K α radiation with a Thermo ARL X'tra powder diffractometer equipped with a Thermo Electron Si(Li) solid state detector. Measurements were performed by 0.05° steps with 10 s of counting time.

Computational Methods. Since the adopted computational approach is fully described elsewhere,^{27,28} only a brief summary will be given here. The various polymorphs were described in terms of rigid molecules interacting through a Buckingham type atom–atom potential with Williams' parameters,²⁹ plus a Coulombic contribution described by atomic charges. This old parameter set is still proved to be among the best for the efficient calculation of polymorph energy rank.^{30,31} The experimental molecular geometry of each polymorph was thus maintained through the calculations, except that all CH distances were foreshortened to 0.98 Å, as specified by the potential model.²⁹

The atomic charges in the model were fitted to the electrostatic potential determined with Density Functional (DFT) calculations on isolated DPA molecules, using the B3LYP/6-31G(d) combination of density functional and basis set.³² As starting molecular geometries for the DFT geometry optimizations, the molecular conformations obtained from the X-ray atomic coordinates were chosen, adding the constraint of a C_{2h} symmetry for α - and β -DPA and D_{2h} symmetry for γ -DPA. Such a choice was made because, as discussed in the structural analysis below, the molecules, although residing on sites with symmetry C_i or C_1 , deviate very little from either C_{2h} (for α - and β -DPA) or D_{2h} (for γ -DPA).

Starting from the experimental crystal structure of each polymorph, the lattice energy was minimized by varying lattice parameters, molecular positions, and orientations. This allowed us to locate the structure at mechanical equilibrium, which corresponds to the local minimum of the potential energy. The effects of temperature T were accounted for with quasi-harmonic lattice dynamics methods,²⁷ by locating the structures at thermodynamical equilibrium, which correspond to the local minima of the Gibbs free energy $G(T)$.

In the tight binding MO approximation, the intermolecular hopping integrals are given by $t_s = \langle \phi | H | \phi_s \rangle$, where H is the one-particle electronic Hamiltonian and ϕ and ϕ_s are the HOMOs (for hole transport) or LUMOs (for electron transport) of the reference molecule and of the molecule at site s , respectively. The integrals are evaluated from the experimental XRD structure through a semiempirical approach based on the INDO/S (intermediate neglect of differential overlap with spectroscopic parametrization, also known as ZINDO) Hamiltonian. For hole transport, this venerable semiempirical method has been proven to give quick estimates of the hopping integrals which agree very well with the experiment and with the results of more sophisticated DFT methods.²⁸

RESULTS

We have recorded the Raman spectra of a high number of DPA crystals prepared by different techniques as explained in the **Sample Preparation** section, giving particular attention to the low wavenumber region, since the lattice modes are the most sensitive to the crystal packing.⁹ In the unpolarized spectra, three clearly different spectral patterns can be easily identified, as shown in **Figure 1**. The spectra have been labeled as α , β , and γ , following the labeling we adopt for the polymorphs.

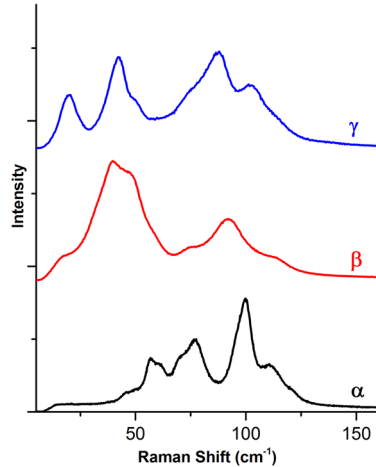


Figure 1. Low wavenumber (THz region) unpolarized Raman spectra of the identified three polymorphs of DPA.

As in the case of 1,1,4,4-tetraphenyl-1,3-butadiene,³³ more subtle but evident and consistent differences are found also in high-frequency (950 – 1450 cm^{-1}) Raman spectra, where the CC stretching and CH bending occur (**Figure 2**).

The α -type spectra are always obtained in the solution-grown samples, and are associated with the well-known $C2/c$ crystal structure.^{15–17} Microribbon crystals give β -type spectra, which are also not reproducibly obtained in crystals grown by sublimation. Crystals grown by the latter method can also exhibit γ -type spectra: a mixture of different polymorphs is

indeed often obtained, and the conditions yielding a single polymorph have not been found.

As shown in **Table 1**, all polymorphs are monoclinic, with factor group C_{2h} and unique screw axis C_2 along the b

Table 1. X-ray Crystal Data (Standard Errors in Parentheses) and Refinement Details

	α -DPA ^a	β -DPA	γ -DPA
chemical formula	C ₂₆ H ₁₈	C ₂₆ H ₁₈	C ₂₆ H ₁₈
temperature	293 K	293 K	300 K
space group	$C2/c$	$P2_1/a$	$P2_1/n$
lattice parameters	$a = 10.683(4)\text{ \AA}$ $b = 13.552(2)\text{ \AA}$ $c = 12.257(2)\text{ \AA}$ $\beta = 90.54(2)^\circ$	$a = 9.4976(10)\text{ \AA}$ $b = 20.413(2)\text{ \AA}$ $c = 10.0843(9)\text{ \AA}$ $\beta = 112.307(9)^\circ$	$a = 9.216(2)\text{ \AA}$ $b = 21.111(5)\text{ \AA}$ $c = 10.041(2)\text{ \AA}$ $\beta = 111.404(4)^\circ$
volume	1774.44 \AA^3	1808.8(3) \AA^3	1818.8(7) \AA^3
Z	4	4	4
density	1.237 g/ cm^3	1.213 g/ cm^3	1.207 g/ cm^3
$F(000)$	696	696	696
theta range	2.958–30.722°	1.93–29.66°	
number of reflections	43684	25950	
reflections with $I > 2\sigma(I)$	2203	3233	
independent reflections	5343	5103	
data/restrains/parameters	2203/0/235	5103/0/307	
GOODF	0.9513	1.077	
final R indices [$I > 2\sigma(I)$]	$R_1 = 0.059$; $wR_2 = 0.059$	$R_1 = 0.0478$; $wR_2 = 0.0457$	$R_1 = 0.0533$; $wR_2 = 0.1367$
R indices (all data)		$R_1 = 0.1273$; $wR_2 = 0.0577$	$R_1 = 0.0857$; $wR_2 = 0.1516$
phenyl/anthracene angle	$68 \pm 1^\circ$	$74 \pm 1^\circ$; $78 \pm 1^\circ$	$89 \pm 1^\circ$

^aFrom ref 16.

crystallographic direction. Accordingly, Raman active modes may have symmetry A_g (polarizations aa , bb , cc , and ac) or B_g (polarizations ab and bc). A detailed description and discussion

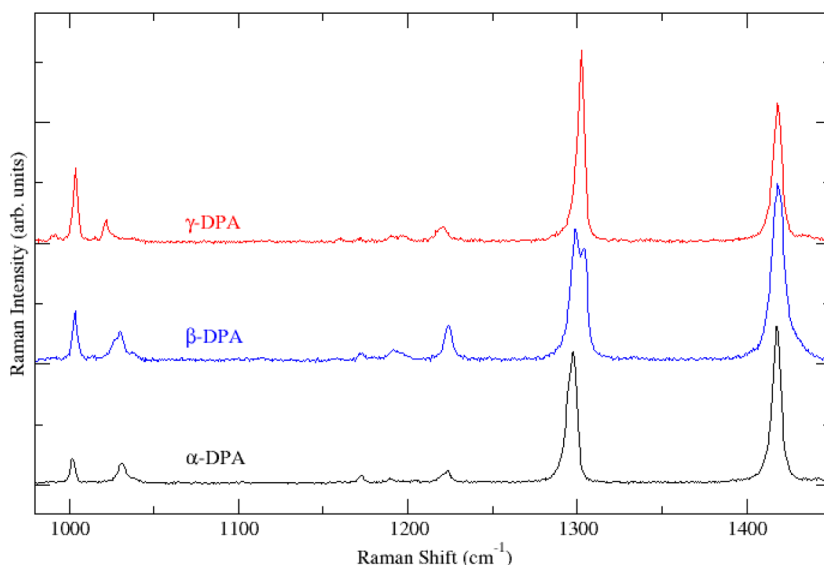


Figure 2. Unpolarized high frequency Raman spectra of the three DPA polymorphs.

of the spectroscopic and structural features of each polymorph will be reported in the following.

Polymorph α . Three X-ray structures of crystalline DPA have been published with complete atomic coordinates,^{15–17} and they all describe the same monoclinic phase, obtained from solution in a variety of solvents. The structural parameters of this phase, which we name polymorph α , also correspond to those given for the sample obtained by zone refining.²

The monoclinic structure¹⁶ has room temperature unit cell parameters $a = 10.683 \text{ \AA}$, $b = 13.552 \text{ \AA}$, $c = 12.257 \text{ \AA}$, and $\beta = 90.54^\circ$ and belongs to the space group $C2/c$ (C_{2h}^0), with four equivalent molecules in the unit cell ($Z = 4$) sitting on inversion sites (Table 1). The asymmetric unit is therefore one-half a molecule. The molecular geometry is C_v , with very small deviations from C_{2h} . The dihedral angle formed by the plane of the anthracene and the phenyl substituent is about 68° .

The unit cell (Figure 3) is nonprimitive, C base-centered. The factor group analysis of the number and the symmetry of

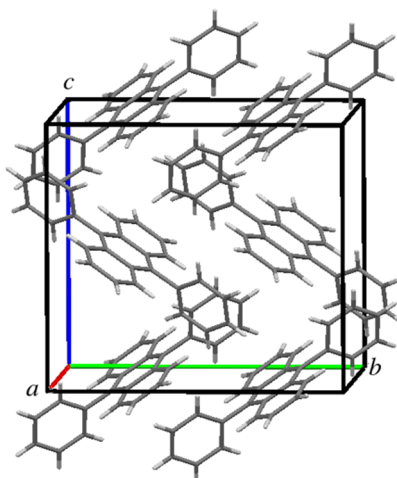


Figure 3. Unit cell of α -DPA.

the vibrational modes must be performed in the reduced primitive cell with $Z = 2$, which has parameters $a' = b' = 8.628 \text{ \AA}$, $c' = c$, $\alpha' = \beta' = 90.33^\circ$, and $\gamma' = 105.503^\circ$. In a vector form, the transformation from conventional to primitive is $\mathbf{a}' = (\mathbf{a} - \mathbf{b})/2$ and $\mathbf{b}' = (\mathbf{a} + \mathbf{b})/2$.

The low-frequency polarized Raman spectra of α -DPA needles grown from toluene solution are shown in Figure 4. The observed crystal face is unknown, and the x,y labels of the polarized spectra correspond to observed extinction directions, which are approximately at 45° from the needle axis (in the used backscattering geometry, z is the direction of the laser beam and of observation). The image of the typical thin-needle morphology which accompanies this lattice phonon spectrum is also given in the right-hand side of Figure 4. The same spectrum is observed in commercial DPA, prior to recrystallization, and is the only one we have found in bulk specimens grown in solution by slow solvent evaporation. Although thin needle crystals characteristically display this spectrum, micro-crystals of different morphology, obtained by slow cooling of the melt or by sublimation, such as those shown in Figure 4, still yield the same spectral features.

In the frame of the rigid molecule approximation (RMA),³⁴ which neglects mixing between lattice and intramolecular modes, out of a total of $6Z - 3 = 9$ lattice modes, six are predicted to be Raman active, of *gerade* symmetry ($3A_g + 3B_g$). However, as in the case of rubrene,³⁵ molecular vibrational modes of low frequency, which involve the phenyl groups attached to the anthracene skeleton, must be present and can couple with lattice vibrations. Indeed the DFT calculations show that three molecular vibrational modes with *gerade* symmetry, suitable for coupling, occur below 150 cm^{-1} . As the site symmetry in the crystal is C_v , each internal mode of *gerade* symmetry splits, according to the C_{2h} factor group, in two components of symmetry A_g and B_g respectively. A total of 12 Raman active modes (lattice and molecular vibrations) is therefore expected in the low-frequency Raman spectra, six belong to A_g symmetry and six to B_g symmetry.

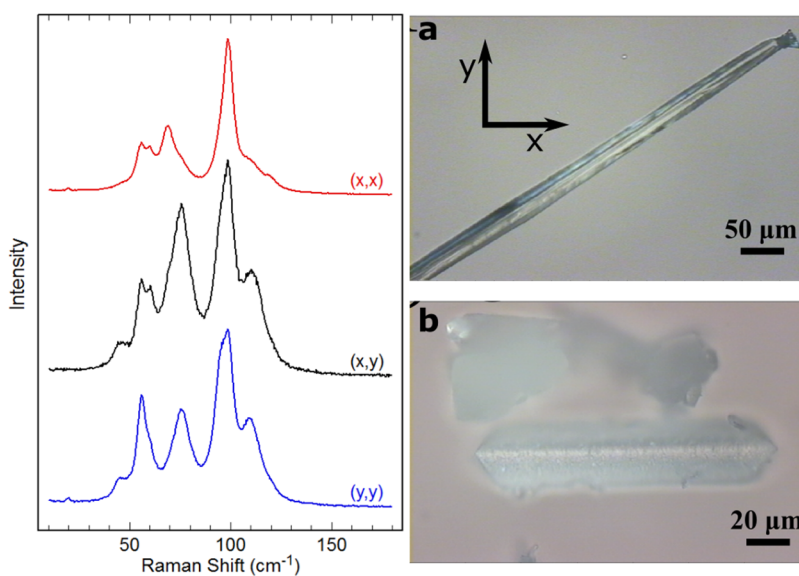


Figure 4. (Left) α -DPA polarized Raman spectra in the low-wavenumber region $10\text{--}150 \text{ cm}^{-1}$. (Right) Optical images of α -DPA samples: (a) needle from slow solvent evaporation and (b) prismatic crystal from low-pressure sublimation. The x,y extinction directions of the crystal are reported.

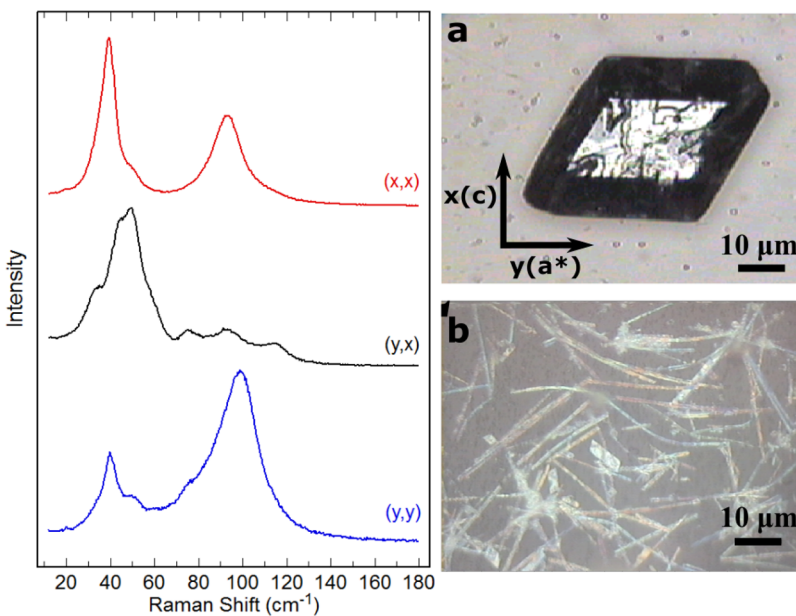


Figure 5. (Left) β -DPA polarized Raman spectra in the low-wavenumber region $10\text{--}150\text{ cm}^{-1}$. The x,y extinction directions coincide with the c and a^* crystal axes, respectively. (Right) Optical images of various β -DPA samples: (a) platelet and (b) microcrystals.

After allowing for residual polarization, each polarized spectrum displays always a number of bands which is higher than six. This implies that we are simultaneously observing both A_g and B_g modes. The exposed face, therefore, cannot be one of the standard faces ab , bc , and ac and must include a nonzero projection of the b axis. A complete list of the frequencies observed below 150 cm^{-1} is reported in the Supporting Information.

Polymorph β . The Raman spectrum of the DPA microcrystals²¹ corresponding to the β -type is shown in Figure 1. Polarized β -type Raman spectra of crystals obtained by vapor deposition (see the Sample Preparation section) are shown in Figure 5 together with the corresponding optical images of the crystals and of the microcrystals, the latter showing the same morphology and dimensions as those given in ref 21. As in the case of the α phase, morphology can vary and the shape of the crystals is never a good diagnostics for the phase identification. Since the spectral pattern (Figure 1) instead is unambiguous, with no overlaps with the spectra of the other phases, a quick Raman scan allowed us to identify and select a number of single crystals from which we have been able to resolve the X-ray structure.

Room temperature cell parameters for this $P2_1/a$ (C_{2h}) structure named polymorph β are $a = 9.4976\text{ \AA}$, $b = 20.413\text{ \AA}$, $c = 10.0843\text{ \AA}$, and $\beta = 112.307^\circ$ (Table 1). The CIF file also reports the X-ray structures at 200 and 105 K. In addition, the Supporting Information compares the simulated powder XRD analysis of the three DPA polymorphs with the experimental one of the microcrystals obtained by the method of ref 21, confirming that they mainly belong to the β phase.

The asymmetric unit contains two half-molecules, sitting on nonequivalent inversion centers at $(0,0,0)$ and $(1/2,0,0)$. The unit cell (Figure 6) therefore contains 4 molecules ($Z = 4$). The dihedral angles between the anthracene backbone and the phenyl groups are slightly different in the two molecules, being about 74° and 78° respectively, and differ from the value found in polymorph α . Also in this case, the deviations from the C_{2h} symmetry are small.

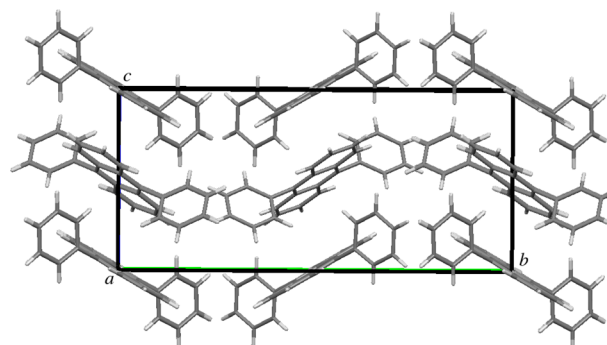


Figure 6. Unit cell of β -DPA.

The XRD analysis shows that β polymorph crystals have a preferential growth in the ac plane. This knowledge allows for a more detailed analysis of the vibrational features of this polymorph. The incident laser light is, in this case, parallel to the monoclinic axis b . As indicated by the XRD, the extinction directions in the ac plane can be identified as $x = c$ and $y = a^*$.

On the basis of selection rules of the C_{2h}^2 crystal space group, out of the $6Z - 3 = 21$ optical lattice modes in the RMA approximation, $12(6A_g + 6B_g)$ are expected to be Raman active. Actually, $3A_g + 3B_g$ are associated with one pair of DPA molecules on C_i site, and the other $3A_g + 3B_g$ are associated with the second pair of DPA on the other nonequivalent C_i site. We expect that the two sets of six modes are strongly overlapped in frequency. By symmetry, when the backscattered radiation from the ac face is analyzed, only the six modes of A_g symmetry can be detected, as the aa , cc , and ac components of the Raman tensor all belong to the totally symmetric representation of the crystal factor group C_{2h} . By allowing the coupling with molecular internal vibrations, as in the case of α -DPA, the number of bands increases, due to the mixing with the totally symmetric contributions of the molecular vibrations. Depending on the specific component of the Raman tensor which is probed in each experiment, different intensity patterns of the A_g bands can be observed in the oriented sample, as a

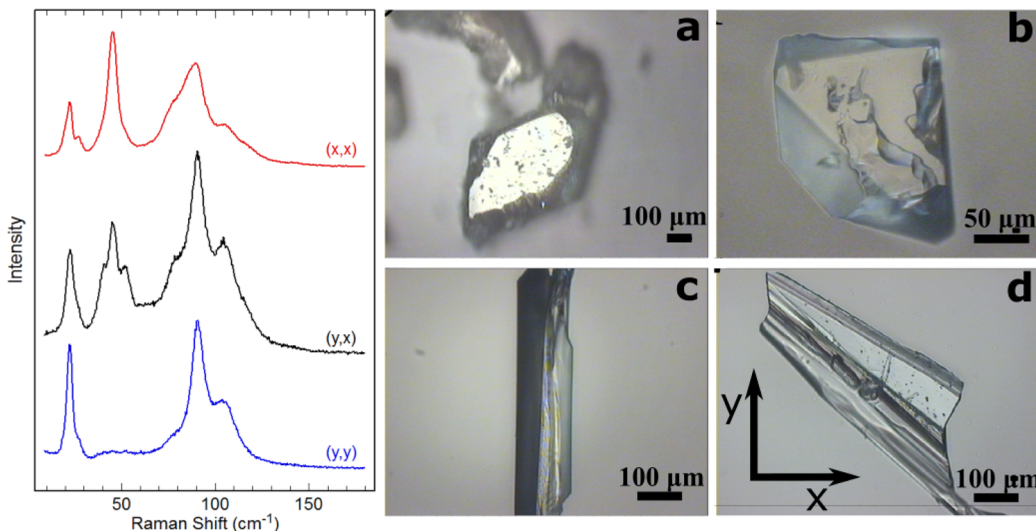


Figure 7. (Left) γ -DPA polarized Raman spectra in the wavenumber region $10\text{--}150\text{ cm}^{-1}$. (Right) Optical images of γ -DPA samples: (a and d) grown by sublimation and (b and c) grown from melt.

result of the relative polarization of incident and scattered light. An example of this is reported in Figure 5, for an oriented platelet. The spectra of the figure have been recorded by collecting the Raman scattering polarized either parallel (a^*a^* , cc) or perpendicular (a^*c) to the excitation. While the total number of bands remains unchanged, the relative intensities change. A complete list of the bands observed below 150 cm^{-1} is given in the Supporting Information.

Also interesting is the intramolecular spectrum of the β form around 1300 cm^{-1} (Figure 2). Here each of the two nonequivalent molecules in the cell gives rise to a distinct intense band, which can be assigned to a vibrational mode largely localized on the phenyl groups and appearing at different frequencies due to the differences in the phenyl dihedral angles. This spectral feature allows for a swift identification of this polymorph also in the energy range of intramolecular vibrations.

Polymorph γ . Polarized Raman spectra of the γ polymorph are shown in Figure 7, together with optical images of the crystals, whose morphology differs considerably. γ -DPA crystals are in general obtained from the melt or by sublimation in mixture with β -DPA. The crystals are very small, but with the help of Raman we have been able to pick up a crystal for the XRD analysis. Crystals coming from a different batch grown by the vapor phase sublimation method²³ also belonged to the γ structure rather than to the β one (see above), showing that it is difficult to find a precise protocol to grow one or the other polymorph.

The γ polymorph crystallizes in the monoclinic group $P2_1/n$ (C_{2h}^2), with four equivalent molecules per unit cell ($Z = 4$), residing in general positions. The asymmetric unit is one molecule. The room temperature cell parameters are $a = 9.216\text{ \AA}$, $b = 21.111\text{ \AA}$, $c = 10.041\text{ \AA}$, and $\beta = 111.404^\circ$ (Table 1). The angle between the anthracene backbone and the phenyl rings is about 89° , and the molecule has no symmetry but approximates a D_{2h} geometry. The unit cell is shown in Figure 8. The CIF file with full structural data is reported in the Supporting Information.

As for the other two polymorphs, the RMA selection rules always predict 12 lattice modes active in Raman ($6A_g + 6B_g$). The XRD analysis shows that the crystallographic face on which

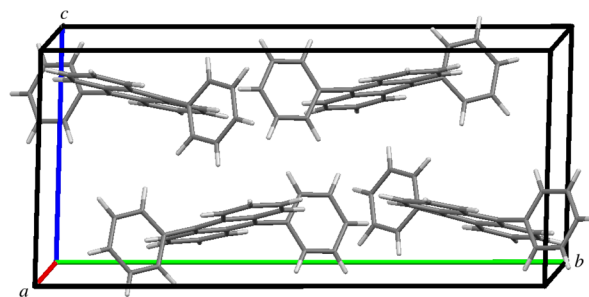


Figure 8. Unit cell of γ -DPA.

the laser light is impinging is not a standard face but certainly contains a nonzero projection of the b axis. In this regard, we therefore expect to be able to observe both A_g and B_g modes, with the latter ones more clearly visible in (x,y) spectrum of Figure 7. Correspondingly, and after allowing for residual polarization, the (x,x) and (y,y) spectra carry information on the totally symmetric modes. The interpretation of this overcrowded spectra is complicated by the mixing between lattice and low-frequency molecular modes, which results in a number of bands higher than expected by RMA, as already remarked in the spectral analysis of the previous polymorphs. A list of the observed low-frequency Raman bands of the γ form is reported in the Supporting Information.

We finally remark that the simple collection of the unit cell parameters by single crystal XRD might lead to confusing the β and γ polymorphs, in view of the similarity of the cell parameters. On the other hand, Raman spectra and/or X-ray powder diffraction pattern are quite different, allowing for a safe identification.

■ POLYMORPHS THERMODYNAMICAL STABILITY

The results of the crystal structure calculations for the DPA polymorphs are reported in Table 2. The lattice parameters, calculated at the potential energy minimum Φ and at the minimum room temperature free energy $G(T)$, are compared to the corresponding XRD data from Table 1. The sixth column of Table 2 also shows that the calculated binding energy of α -DPA matches the closest experimental equivalent,

Table 2. Experimental (Standard Errors in Parentheses) and Computed Lattice Parameters and Binding Energies of DPA Polymorphs

		<i>a</i> (Å)	<i>b</i> (Å)	<i>c</i> (Å)	β (deg)	volume (Å ³)	energy ^a (kJ/mol)	RMSD ₂₀ ^b (Å)
α -DPA	exptl	10.683(4)	13.552(2)	12.257(2)	90.54	1774.44	-156.9 ± 4.2	
	min ϕ	10.5214	13.6036	12.2670	91.244	1755.35	-134.7	0.156
	min G	10.6108	13.6130	12.4076	91.417	1791.67	-153.3	0.150
β -DPA	exptl	9.4976(10)	20.413(2)	10.0843(9)	112.307	1808.8(3)		
	min ϕ	9.5210	20.3976	9.9999	112.257	1797.34	-129.5	0.056
	min G	9.5713	20.5196	10.0282	111.665	1830.40	-149.2	0.080
γ -DPA	exptl	9.216(2)	21.111(5)	10.041(2)	111.404(4)	1818.8(7)		
	min ϕ	9.2246	20.9321	10.2069	113.798	1803.27	-128.4	0.089
	min G	9.2904	20.9538	10.2487	113.626	1827.89	-147.1	0.126

^aThe experimental energy is $\Delta_{\text{subl}}H$, from ref 36. ^bMeasure of the distance between calculated and experimental structure. See text.

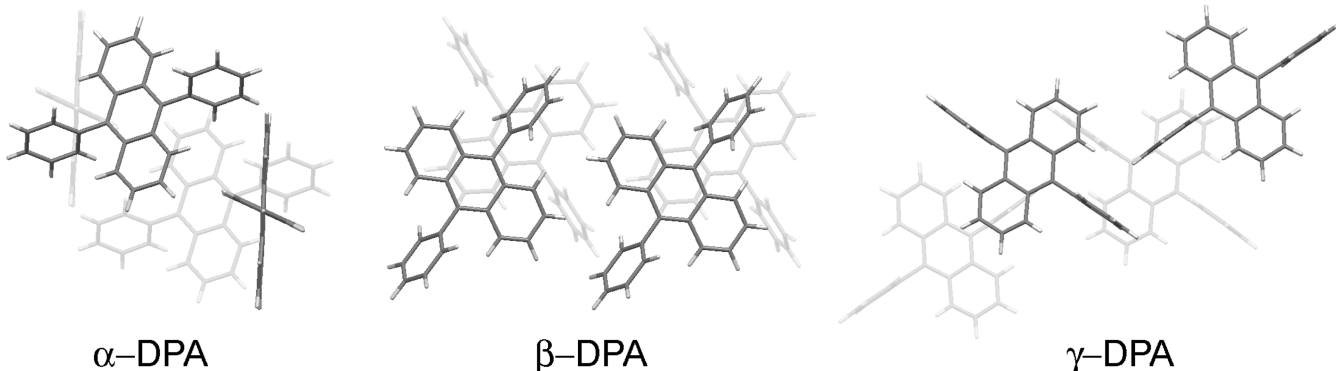


Figure 9. Pair molecular arrangement in DPA polymorphs.

namely the sublimation enthalpy.³⁶ This indicates that the potential model correctly reproduces the experimental intermolecular binding, giving confidence to the computed energy values for β - and γ -DPA.

The computed unit cell volumes at minimum Φ are systematically smaller than the experimental ones, and this is expected as no thermal effects are included. The lattice expands once these effects are accounted for, yielding volumes at minimum $G(T)$ larger than the experimental ones.

As an efficient and compact measure of the agreement between structures, we have used the distance comparison method.^{37,38} For each structure of interest, we list all the interatomic distances between a reference molecule and at least 20 neighboring molecules in a spherical coordination shell. Pairs of structures are then compared by computing RMSD₂₀, which is the root-mean-square deviation between their lists of distances. Very small RMSD₂₀ indicate that the interatomic distances in the two structures are essentially the same and, therefore, that the structures are very similar. For all DPA polymorphs, the Table 2 last column RMSD₂₀ between calculated and experimental structures is well below 0.2 Å, a value which, for pairs of X-ray structures, would certainly indicate that they coincide.³⁸

It should be pointed out that the agreement with the experiments has been found excellent only by employing in the calculations the molecular geometry as given by the XRD measurements. The attempt to use the optimized DFT geometry leads to structures with large deviations from the experiments (results not shown), especially for the α polymorph. In fact, the main difference between calculated and experimental geometries involves the torsional angles between the anthracene skeleton and the phenyl groups, which are 68° in α -DPA and 74° or 78° in β -DPA versus ≈75° in the

corresponding C_{2h} DFT geometry and 89° in γ -DPA versus 90° in the D_{2h} DFT geometry. This is a strong indication of the connection between the molecular conformational changes and the different crystal packing in the three polymorphs.^{11,38}

The α polymorph turns out to be the most stable, corresponding to the deepest minimum of the potential energy Φ and also of the free energy $G(T)$. The β polymorph comes next, and the γ polymorph is the least stable. Following the rule of thumb for relative polymorph stability, α -DPA is also the most dense structure, and thus, predictably, the most stable. Experimental and computed densities, in fact, both decrease in the order of α , β , and γ . The energy difference between β - and γ -DPA (2.02 kJ/mol) is minimal, and this may explain the difficulties of obtaining the two polymorphs separately.

By examining the free energy curves $G(T)$ of the three polymorphs (Figure S2), we have found that, although the differences between the free energy of α -DPA and β or γ -DPA decrease with T , the curves never cross in the whole temperature range up to the melting point so that the stability ranking α , β , and γ is maintained. Therefore, at least from the computational point of view, the three crystal phases are in a monotropic relationship,¹¹ that means that only one of the phases (α -DPA) is thermodynamically stable at all temperatures.

CRYSTAL PACKING AND MOBILITY CHANNELS

All DPA polymorphs crystallize in the monoclinic system, with four molecules per unit cell. As in the case of rubrene,²⁷ or tetraphenylbutadiene,³⁹ great importance in the different crystal packing can be ascribed to the position and orientation of the phenyl groups with respect to the π -conjugated backbone. As we have already mentioned, the orientation of the phenyl

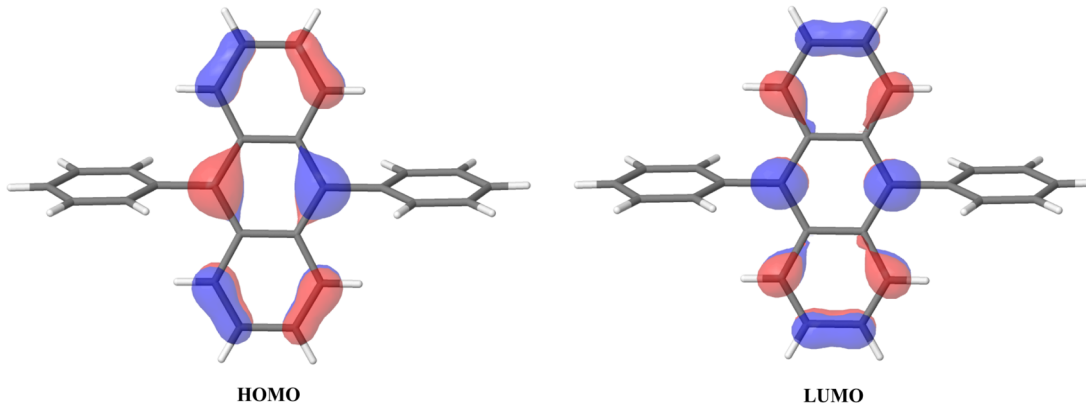


Figure 10. HOMO and LUMO of isolated DPA, as obtained from DFT calculations.

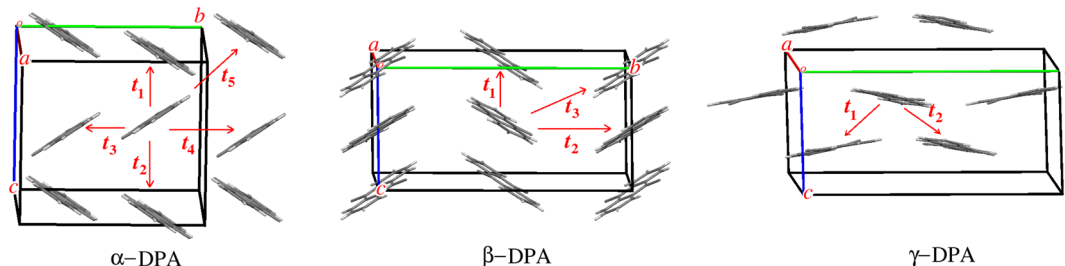


Figure 11. Packing and definition of the nearest-neighbor hopping integrals in the three DPA polymorphs. The DPA molecules are viewed from the anthracene long axis, and the phenyl groups have been omitted for the sake of clarity.

groups differs in the three polymorphs, and their steric hindrance yields different orientations and arrangements between pairs of molecules. This is clearly illustrated in Figure 9, where the molecular pairs have been chosen on the basis of the strongest interactions within each polymorph, as found by atom–atom potentials.

As mentioned in the Introduction, α -DPA exhibits a good single crystal carrier mobility.² The mobility values are lower than those of rubrene, but in the latter, only hole mobility has been observed, whereas in DPA comparable values of hole and electron mobility have been observed. Since both rubrene and DPA have pendant phenyl groups, and it has been speculated² that phenyl overlap may contribute to the mobility, it is useful to perform quantum mechanical calculations to investigate the DPA mobility channels and to compare them with the corresponding ones of rubrene and anthracene.

Figure 10 shows DPA highest occupied and lowest empty molecular orbitals (HOMO and LUMO), computed by DFT, from which the valence and conduction bands originate. In both cases, there is no appreciable electron density on the phenyl groups. The same is true for the HOMO-1 orbital, whereas the LUMO+1 orbital has some electron density on the phenyls but is separated by about 1 eV from the LUMO. To start with, it is therefore plausible to postulate that the carrier transport occurs throughout the anthracene backbone.

Figure 11 reports the packing and the definition of the relevant hopping integral of the three polymorphs. The phenyl groups have been omitted for clarity. For the α phase, the mobility has been measured along the c^* direction,² roughly corresponding to the direction of t_1 and t_2 hopping integrals. The partial overlap between the anthracene backbone is evident in this case. The comparison between the panels in the figure clearly indicates the quite different reciprocal orientation of the DPA molecules, as already discussed in connection with Figure

9. The central panel of Figure 11 also shows the rather unusual overlap between the DPA molecules along c : the molecules lie face-to-face but twisted by $\sim 60^\circ$.

A quick way to investigate the mobility channels of organic semiconductors is to calculate the HOMO–HOMO and LUMO–LUMO hopping integrals. Since we have verified that the HOMO–HOMO hopping integrals calculated by the INDO/S method give results comparable to those obtained by more sophisticated quantum-chemical calculations,^{27,28} we have adopted this method also in the present case. In any case, what is important is the relative comparison between the hopping integrals calculated by the same method.

In Table S2, we report the calculated integrals of the DPA polymorphs compared with those of anthracene and rubrene, all computed at the experimental room temperature structure.

We first discuss hole (HOMO) hopping integrals. The highest t values of α -DPA compare well with those of anthracene, and are lower than that of rubrene, in agreement with the observed trend of the measured hole mobilities.² Therefore, we confirm that the role of the phenyl groups is marginal in the hole mobility of DPA and rubrene. The highest hole hopping integrals in α -DPA are approximately along the a and c axes, but one relatively high and one small integral alternate along these directions. Although mobility has been measured along c^* , one expects two-dimensional transport. In the case of β -DPA, instead Table S2 predicts, similarly to rubrene,²⁷ a quasi-one-dimensional transport (along c). Finally, γ -DPA seems to be the less favorable polymorph for the transport properties. When considering the electron (LUMO) hopping integrals, one finds that in the case of DPA such values are considerably lower than those for hole hopping. This is rather surprising, as the α -DPA hole and electron mobilities are comparable.² One might suppose that at least in this case the phenyl groups may contribute to the transport. On the other

hand, whereas the INDO/S calculations of hopping integrals have been shown to agree very well with experiment and different calculations,^{27,28} such an agreement has not been so far verified for the electron hopping. More sophisticated calculations, as well as careful measurements of the mobilities of the different DPA phases are needed, but this goes beyond the aim of the present paper.

■ DISCUSSION AND CONCLUSIONS

Although polymorphism is widely encountered in organic compounds, only recently has the scientific community demonstrated a sensitivity to its importance in the field of materials for applications in electronics. Certainly, the more ways are sought to grow a given material in suitable crystalline forms, the more solid phases are found, and DPA seems to fit entirely in this scheme. Next to the well-known α phase, we have discovered two new polymorphs, β -DPA and γ -DPA. In this achievement, a fundamental and invaluable help comes from Raman spectroscopy in the THz frequency region, as it allows one to quickly discover and sort out crystallites of different polymorphs to submit to X-ray investigation.

As calculations and experiments indicate that the α phase is the thermodynamically stable one, no precaution should be taken to preserve it in devices and applications, once it has been obtained. Instead, the β and γ phases could be metastable. However, a kinetically controlled transformation between them and/or to the α phase is made unlikely by the large molecular motions that such a transformation would require. Interestingly, the three polymorphs can form in very similar conditions, although the observation that β and γ are obtained in “fast processes” is a further indication that their formation is kinetically controlled. This kinetic control also explains why it has not been possible to find precise conditions to obtain crystals of either the β or the γ phase. The β polymorph, on the other hand, has been obtained in microstructures. Note that in ref 19, DPA so-called nanostructures were found to have the same structure as the α polymorphs. However, those were obtained in the presence of a surfactant, not used in our procedure.²¹

The reported mobilities of DPA have been measured on single crystals.² On the other hand, working electronic devices like transistors are generally based on thin films of the active organic material grown on a suitable surface (organic thin film transistors, OTFT). As in the case of pentacene, thin films may have a structure different from those of the bulk, depending on the growth conditions and surface.⁴⁰ The high vacuum molecular beam deposition may favor the kinetically controlled polymorph, besides eventual additional thin-film polymorphs, as it has been recently shown with the help of Raman spectroscopy.⁴¹ The present study indicates that only α -type or β -type films are likely to display good transport properties, and in any case, it paves the way to a detailed *in situ* investigation of DPA-based OTFT.

■ ASSOCIATED CONTENT

Supporting Information

The Supporting Information is available free of charge on the ACS Publications website at DOI: [10.1021/acs.jpcc.5b11115](https://doi.org/10.1021/acs.jpcc.5b11115).

Frequencies and polarization of the Raman bands observed below 150 cm⁻¹; powder XRD of microcrystals; computed free energy (G) as a function of temperature;

and computed hopping integrals of the three polymorphs ([PDF](#))

Crystallographic data for β -DPA at three temperatures ([CIF](#))

Crystallographic data for γ -DPA at room temperature ([CIF](#))

■ AUTHOR INFORMATION

Corresponding Authors

*E-mail: elisabetta.venuti@unibo.it.

*E-mail: alberto.girlando@unipr.it.

Notes

The authors declare no competing financial interest.

■ ACKNOWLEDGMENTS

The Laboratorio di Strutturistica “Mario Nardelli” of the Dipartimento di Chimica at the University of Parma is gratefully acknowledged for providing diffraction facilities. Part of the work by T.S. was performed at Bell Laboratories, Alcatel-Lucent, Murray Hill, NJ (U.S.A.). This work has been supported by the Italian Ministry of University and Research (M.I.U.R.) under the project PRIN-2010ERFKXL.

■ REFERENCES

- (1) Dong, H.; Fu, X.; Liu, J.; Wang, Z.; Hu, W. 25th Anniversary Article: Key Points for High-Mobility Organic Field-Effect Transistors. *Adv. Mater.* **2013**, *25*, 6158–6183.
- (2) Tripathi, A. K.; Heinrich, M.; Siegrist, T.; Pflaum, J. Growth and Electronic Transport in 9,10-Diphenylanthracene Single Crystals-An Organic Semiconductor of High Electron and Hole Mobility. *Adv. Mater.* **2007**, *19*, 2097–2101.
- (3) Fujiwara, Y.; Ozawa, R.; Onuma, D.; Suzuki, K.; Yoza, K.; Kobayashi, K. Double Alkylene-Strapped Diphenylanthracene as a Photostable and Intense Solid-State Blue-Emitting Material. *J. Org. Chem.* **2013**, *78*, 2206–2212.
- (4) Troisi, A.; Orlandi, G. Band Structure of the Four Pentacene Polymorphs and Effect on the Hole Mobility at Low Temperature. *J. Phys. Chem. B* **2005**, *109*, 1849–1856.
- (5) Matsukawa, T.; Yoshimura, M.; Sasai, K.; Uchiyama, M.; Yamagishi, M.; Tominari, Y.; Takahashi, Y.; Takeya, J.; Kitaoka, Y.; Mori, Y.; et al. Growth of Thin Rubrene Single Crystals from 1-propanol Solvent. *J. Cryst. Growth* **2010**, *312*, 310–313.
- (6) Bergantin, S.; Moret, M. Rubrene Polymorphs and Derivatives: The Effect of Chemical Modification on the Crystal Structure. *Cryst. Growth Des.* **2012**, *12*, 6035–6041.
- (7) Schweicher, G.; Olivier, Y.; Lemaur, V.; Geerts, Y. H. What Currently Limits Charge Carrier Mobility in Crystals of Molecular Semiconductors? *Isr. J. Chem.* **2014**, *54*, 595–620.
- (8) Yuan, Y.; Giri, G.; Ayzner, A. L.; Zoombelt, A. P.; Mannsfeld, S. C. B.; Chen, J.; Nordlund, D.; Toney, M. F.; Huang, J.; Bao, Z. Ultra-high Mobility Transparent Organic Thin Film Transistors Grown by an Off-centre Spin-coating Method. *Nat. Commun.* **2014**, *5*, 3005.
- (9) Brillante, A.; Bilotti, I.; Della Valle, R. G.; Venuti, E.; Masino, M.; Girlando, A. Characterization of Phase Purity in Organic Semiconductors by Lattice Phonon Confocal Raman Mapping: Application to Pentacene. *Adv. Mater.* **2005**, *17*, 2549–2553.
- (10) Ando, M.; Kehoe, T. B.; Yoneya, M.; Ishii, H.; Kawasaki, M.; Duffy, C. M.; Minakata, T.; Phillips, R. T.; Sirringhaus, H. Evidence for Charge-Trapping Inducing Polymorphic Structural-Phase Transition in Pentacene. *Adv. Mater.* **2015**, *27*, 122–129.
- (11) Bernstein, J. *Polymorphism in Molecular Crystals*; Clarendon Press: Oxford, 2002.
- (12) Brillante, A.; Bilotti, I.; Della Valle, R. G.; Venuti, E.; Girlando, A. Probing Polymorphs of Organic Semiconductors by Lattice Phonon Raman Microscopy. *CrystEngComm* **2008**, *10*, 937–946.

- (13) Pfattner, R.; Mas-Torrent, M.; Bilotti, I.; Brillante, A.; Milita, S.; Liscio, F.; Biscarini, F.; Marszalek, T.; Ulanski, J.; Nosal, A.; et al. High-Performance Single Crystal Organic Field-Effect Transistors Based on Two Dithiophene-Tetrathiafulvalene (DT-TTF) Polymorphs. *Adv. Mater.* **2010**, *22*, 4198–4203.
- (14) Hiszpanski, A. M.; Loo, Y.-L. Directing the Film Structure of Organic Semiconductors via Post-deposition Processing for Transistor and Solar Cell Applications. *Energy Environ. Sci.* **2014**, *7*, 592–608.
- (15) Adams, J. M.; Ramdas, S. The Crystal Structure of Solution-grown 9,10-Diphenylanthracene. A Combined Computational and X-ray Study. *Acta Crystallogr., Sect. B: Struct. Crystallogr. Cryst. Chem.* **1979**, *35*, 679–683.
- (16) Langer, V.; Becker, H.-D. Crystal Structure of 9,10-Diphenylanthracene, $(C_6H_5)(C_{14}H_8)(C_6H_5)$. *Z. Kristallogr.* **1992**, *199*, 313–315.
- (17) Munakata, M.; Wu, L. P.; Kuroda-Sowa, T.; Maekawa, M.; Suenaga, Y.; Ohta, T.; Konaka, H. Construction of the Multidecker Anthracene-Silver(I) System by Intramolecular - Interactions. *Inorg. Chem.* **2003**, *42*, 2553–2558.
- (18) Sloan, G. Personal communication to Thoms, J. M., reported in ref 15.
- (19) Zhang, X.; Yuan, G.; Li, Q.; Wang, B.; Zhang, X.; Zhang, R.; Chang, J. C.; Lee, C.; Lee, S. Single-Crystal 9,10-Diphenylanthracene Nanoribbons and Nanorods. *Chem. Mater.* **2008**, *20*, 6945–6950.
- (20) Yang, B.; Xiao, J.; Wong, J. I.; Guo, J.; Wu, Y.; Ong, L.; Lao, L.; Boey, F.; Zhang, H.; Yang, H. Y.; Zhang, Q. Shape-Controlled Micro/Nanostructures of 9,10-Diphenylanthracene (DPA) and Their Application in Light-Emitting Devices. *J. Phys. Chem. C* **2011**, *115*, 7924–7927.
- (21) Zhang, X.; Zhang, X.; Wang, B.; Zhang, C.; Chang, J. C.; Lee, C. S.; Lee, S.-T. One- or Semi-Two-Dimensional Organic Nanocrystals Induced by Directional Supramolecular Interactions. *J. Phys. Chem. C* **2008**, *112*, 16264–16268.
- (22) Kloc, C.; Siegrist, T.; Pflaum, J. *Springer Handbook of Crystal Growth*; Dhanaraj, G., Byrappa, K., Prasad, V., Dudley, M., Eds., Springer: Berlin, 2010; pp 845–867.
- (23) Laudise, R. A.; Kloc, Ch.; Simpkins, P. G.; Siegrist, T. Physical Vapor Growth of Organic Semiconductors. *J. Cryst. Growth* **1998**, *187*, 449–454.
- (24) Betteridge, P. W.; Carruthers, J. R.; Cooper, R. I.; Prout, K.; Watkin, D. J. CRYSTALS version 12 contains a modern crystallographic user interface, and novel strategies that incorporate chemical knowledge and crystallographic guidance into the crystal structure analysis software. *J. Appl. Crystallogr.* **2003**, *36*, 1487–1487.
- (25) Burla, M. C.; Caliandro, R.; Camalli, M.; Carrozzini, B.; Casciaro, G. L.; De Caro, L.; Giacovazzo, C.; Polidori, G.; Spagna, R. SIR2004: An Improved Tool for Crystal Structure Determination and Refinement. *J. Appl. Crystallogr.* **2005**, *38*, 381–338.
- (26) Sheldrick, G. M. *SHELXL97*, Program for the Crystal StructureRefinement; Univ. of Gottingen: Germany, 1993.
- (27) Girlando, A.; Grisanti, L.; Masino, M.; Bilotti, I.; Brillante, A.; Della Valle, R. G.; Venuti, E. Peierls and Holstein Carrier-phonon Coupling in Crystalline Rubrene. *Phys. Rev. B: Condens. Matter Mater. Phys.* **2010**, *82*, 035208.
- (28) Girlando, A.; Grisanti, L.; Masino, M.; Brillante, A.; Della Valle, R. G.; Venuti, E. Interaction of Charge Carriers with Lattice and Molecular Phonons in Crystalline Pentacene. *J. Chem. Phys.* **2011**, *135*, 084701.
- (29) Williams, D. E. Improved Intermolecular Force Field for Crystalline Hydrocarbons Containing Four- or Three-coordinated Carbon. *J. Mol. Struct.* **1999**, *485–486*, 321–447.
- (30) Grančič, P.; Bylsma, R.; Meekes, H.; Cuppen, H. M. Evaluation of All-Atom Force Fields for Anthracene Crystal Growth. *Cryst. Growth Des.* **2015**, *15*, 1625–1633.
- (31) Nyman, J.; Day, G. M. Static and Lattice Vibrational Energy Differences Between Polymorphs. *CrystEngComm* **2015**, *17*, 5154–5165.
- (32) Frisch, M. J.; Trucks, G. W.; Schlegel, H. B.; Scuseria, G. E.; Robb, M. A.; Cheeseman, J. R.; Montgomery, J. A., Jr.; Vreven, T.; Kudin, K. N.; Burant, J. C. et al. *Gaussian03*, revision D.02; Gaussian Inc.: Wallingford, CT, 2004.
- (33) Bacchi, A.; Bilotti, I.; Brillante, A.; Crocco, D.; Della Valle, R. G.; Girlando, A.; Masino, M.; Pelagatti, P.; Venuti, E. Raman and X-ray Investigation of Polymorphism in 1,1,4,4-Tetraphenylbutadiene. *J. Raman Spectrosc.* **2013**, *44*, 905–908.
- (34) Ranzieri, P.; Girlando, A.; Tavazzi, S.; Campione, M.; Raimondo, L.; Bilotti, I.; Brillante, A.; Della Valle, R. G.; Venuti, E. Polymorphism and Phonon Dynamics in α -Quaterthiophene. *ChemPhysChem* **2009**, *10*, 657–663.
- (35) Venuti, E.; Bilotti, I.; Della Valle, R. G.; Brillante, A.; Ranzieri, P.; Masino, M.; Girlando, A. Polarized Raman Spectra of a Rubrene Single Crystal. *J. Phys. Chem. C* **2008**, *112*, 17416–17422.
- (36) Roux, M. V.; Temprado, M.; Chickos, J. S.; Nagano, Y. Critically Evaluated Thermochemical Properties of Polycyclic Aromatic Hydrocarbons. *J. Phys. Chem. Ref. Data* **2008**, *37*, 1855–1996.
- (37) Chisholm, J.; Motherwell, W. D. S. COMPACK: A Program for Identifying Crystal Structure Similarity Using Distances. *J. Appl. Crystallogr.* **2005**, *38*, 228–231.
- (38) Cruz-Cabeza, A. J.; Bernstein, J. Conformational Polymorphism. *Chem. Rev.* **2014**, *114*, 2170–2191.
- (39) Bacchi, A.; Brillante, A.; Crocco, D.; Chierotti, M. R.; Della Valle, R. G.; Girlando, A.; Masino, M.; Pelagatti, P.; Venuti, E. Exploration of the Polymorph Landscape for 1,1,4,4-Tetraphenyl-1,3-butadiene. *CrystEngComm* **2014**, *16*, 8205–8213.
- (40) Ruiz, R.; Choudhary, D.; Nickel, B.; Toccoli, T.; Chang, K. C.; Mayer, A. C.; Clancy, P.; Blakely, J. M.; Headrick, R. L.; Iannotta, S.; Malliaras, G. G. Pentacene Thin Film Growth. *Chem. Mater.* **2004**, *16*, 4497–4508.
- (41) Brillante, A.; Bilotti, I.; Della Valle, R. G.; Venuti, E.; Girlando, A.; Masino, M.; Liscio, F.; Milita, S.; Albonetti, C.; D'Angelo, P.; et al. Structure and Dynamics of Pentacene on SiO_2 : From Monolayer to Bulk Structure. *Phys. Rev. B: Condens. Matter Mater. Phys.* **2012**, *85*, No. 195308.